Steel and Composite Structures, *Vol. 29, No. 5 (2018) 579-590*
DOI: https://doi.org/10.12989/scs.2018.29.5.579

Size-dependent vibration and electro-magneto-elastic bending responses of sandwich piezomagnetic curved nanobeams

Mohammed Arefi [1a] and Ashraf M. Zenkour [*2,3]

[1] *Faculty of Mechanical Engineering, Department of Solid Mechanics, University of Kashan, Kashan 87317-51167, Iran*
[2] *Department of Mathematics, Faculty of Science, King Abdulaziz University, Jeddah 21589, Saudi Arabia*
[3] *Department of Mathematics, Faculty of Science, Kafrelsheikh University, Kafrelsheikh 33516, Egypt*

(*Received January 22, 2018, Revised September 29, 2018, Accepted November 17, 2018*)

Abstract. Size-dependent free vibration responses and magneto-electro-elastic bending results of a three layers piezomagnetic curved beam rest on Pasternak's foundation are presented in this paper. The governing equations of motion are derived based on first-order shear deformation theory and nonlocal piezo-elasticity theory. The curved beam is containing a nanocore and two piezomagnetic face-sheets. The piezomagnetic layers are imposed to applied electric and magnetic potentials and transverse uniform loadings. The analytical results are presented for simply-supported curved beam to study influence of some parameters on vibration and bending results. The important parameters are spring and shear parameters of foundation, applied electric and magnetic potentials, nonlocal parameter and radius of curvature of curved beam. It is concluded that the increase in radius of curvature tends to an increase in the stiffness of curved beam and consequently natural frequencies increase and bending results decrease. In addition, it is concluded that with increase of nonlocal parameter of curved beam, the stiffness of structure is decreased that leads to decrease of natural frequency and increase of bending results.

Keywords: curved sandwich nanobeam; piezomagnetic face-sheets; Pasternak's foundation; radius of curvature; nonlocal parameter

1. Introduction

In this study, the governing equations of motion for a sandwich curved nanobeam are derived. The model is including an elastic core and two integrated piezomagnetic face-sheets as sensor and actuator. The integrated face-sheets can be utilized as sensor and actuator to control deflection or stress of curved beam. The piezomagnetic face-sheets are loaded to applied electric and magnetic potentials to measure or control the electro-mechanical parameter such as displacement, rotation, electric and magnetic potentials distributions. These behaviors have been extensively studied by various researchers for beam and plates. Our study indicates that this subject has not been applied for curved structures such as curved beam. The literature review is presented to mention the necessity of this subject.

Sun and Tong (2001) investigated vibration control of a beam integrated with curved piezoelectric fibers. Once again, Sun and Tong (2002) discussed an analytical method to investigate the effect of debonding of piezoelectric actuator/sensor patches. Shi (2005) presented bending response of functionally graded material (FGM) piezoelectric curved actuator under an external voltage by using theory of piezo-elasticity. The influence of power index of FGM has been investigated on the obtained results which have been approved by comparison with finite element method. Ebrahimi and Beni (2016) presented the free vibrations of a short cylindrical piezoelectric nanotube are studied based on the consistent couple stress theory and using the shear deformable cylindrical theory. Mohammadimehr and Shahedi (2016) presented the nonlinear magneto-electro-mechanical free vibration behavior of rectangular double-bonded sandwich micro-beams based on the modified strain gradient theory. Amar *et al*. (2018) investigated a new plate formulation and a modified couple stress theory to introduce a variable length scale parameter and discuss the static and dynamic of FG microplates.

Koutsawa and Daya (2007) investigated static and free vibration behaviors of laminated glass beam rest on visco-Pasternak foundation. For free vibration analysis, finite element method has been used. Kuang *et al*. (2007) investigated static behavior of a circular piezoelectric curved beam. Bending response of a FG piezoelectric curved beam under an electric potential has been presented by Shi and Zhang (2008). Also, Susanto (2009) discussed piezoelectric curved beams due to a model including computation of natural frequencies, mode shapes and transfer function formulation using the distributed transfer function method.

Zhou *et al*. (2016) studied transient response analysis of piezoelectric curved beam. The influence of surface effect has been employed on electromechanical behavior of a piezoelectric curved nanobeam under electromechanical

*Corresponding author, Ph.D., Professor,
E-mail: zenkour@kau.edu.sa; zenkour@sci.kfs.edu.eg
[a] Ph.D., E-mail: arefi@kashanu.ac.ir

ISSN: 1229-9367 (Print), 1598-6233 (Online)

loadings by Yan and Jiang (2011) based on Euler–Bernoulli curved beam theory. They mentioned some usefulness of the current model as nano/switches/actuators for control of displacement. Hajianmaleki and Qatu (2013) employed vibration response of composite beams using various analytical and numerical methods. Arefi and Rahimi (2014) studied piezomagnetic response of thicker FG shell of revolution with the aid of tensor curvilinear coordinates. Kakar and Kakar (2014, 2015) introduced a combined effect of electric field, magnetic field and thermal field on edge wave propagating in a non-homogeneous orthotropic granular half space and a homogeneous isotropic prestressed plate.

Arslan and Usta (2014) employed theory of elasticity for electrical and mechanical behaviors of curved bars. Bahadur *et al*. (2018) studied an analytical solution for the static analysis of laminated FG and sandwich singly and doubly curved panels on the rectangular plan-form. Rahmani *et al*. (2017) presented a new model based on nonlocal higher-order theory to study the size-effect on the bending of sandwich nanobeams with a compliance core. Arefi (2015) presented elastic solution of a FG curved beam with various cross sections. Zhou *et al*. (2010) presented piezoelectric response of curved nanobeams with variable curvature as an element of electromechanical systems. Arefi and Zenkour (2017a, b, d, e) studied on the influence of applied electric and magnetic potentials on the free vibration and bending results of sandwich nanoplates and nanobeams. Wave propagation analysis of nanorod model was studied based on couple stress and surface elasticity theory by Arefi and Zenkour (2017c, f). Shao *et al*. (2016) analyzed transient response of composite laminated curved beams with general lamination and boundary conditions using Laplace transformation. They studied the influence of shear deformation, rotary inertia, various laminations and boundary conditions on the transient responses of the curved beam. Ebrahimi and Barati (2017) investigate buckling problem of a curved FG nanobeam. The problem has been formulated due to strain gradient theory and a higher-order refined beam theory. Finally, the governing equations have been solved for simply-supported and clamped-clamped beams. Pydah and Sabale (2017) studied static response of a FG circular curved beam via Euler–Bernoulli theory.

In this paper, the first-order theory is employed to obtain governing equations of motion for a three-layer curved nanobeam integrated with piezomagnetic face-sheets. The electric and magnetic potential is assumed as combination of a linear function along the thickness direction that reflects applied electric and magnetic potentials and a cosine function that reflects electric and magnetic boundary conditions. Combination of curved nanobeam problem with piezomagnetic materials leads to an important and novel subject that can be applicable in electro-mechanical systems as sensor and actuator for control of deflections or stresses.

2. Basic relations

In this section, the formulation of a curved beam is presented. Fig. 1 plots the schematic of the present three-layer curved nanobeam.

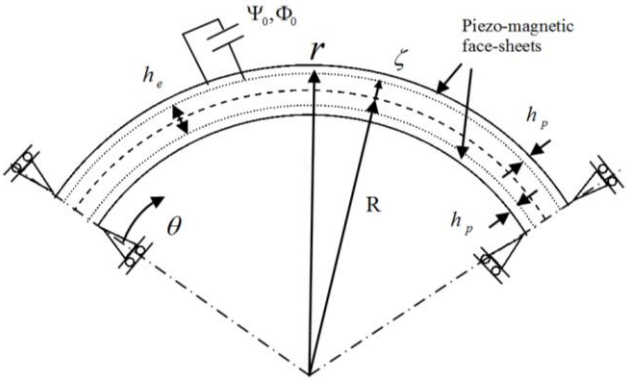

Fig. 1 The schematic of a three-layer curved nanobeam

Two displacement components are considered including radial and circumferential displacements. First-order shear deformation theory is used for circumferential displacement.

According to this theory, two displacements can be represented by (Shi and Zhang 2008, Arefi and Rahimi 2014)

$$\begin{aligned} u_r(r,\theta) &= u_r(\theta), \\ u_\theta(r,\theta) &= u_\theta(\theta) + \zeta\chi(\theta), \end{aligned} \tag{1}$$

in which $\zeta = r - R$. The strain-displacement equations based on polar coordinate are represented as

$$\begin{aligned} \varepsilon_r &= \frac{\partial u_r}{\partial r} = 0, \\ \varepsilon_\theta &= \frac{u_r}{r} + \frac{1}{r}\frac{\partial u_\theta}{\partial \theta} = \frac{u_r}{R+\zeta} + \frac{1}{R+\zeta}\frac{du_\theta}{d\theta} + \frac{\zeta}{R+\zeta}\frac{d\chi}{d\theta}, \\ \gamma_{r\theta} &= \frac{1}{r}\frac{\partial u_r}{\partial \theta} + \frac{\partial u_\theta}{\partial r} - \frac{u_\theta}{r} \\ &= \frac{1}{R+\zeta}\frac{du_r}{d\theta} + \chi - \frac{u_\theta}{R+\zeta} - \frac{\zeta}{R+\zeta}\chi. \end{aligned} \tag{2}$$

In this stage, the stress components including circumferential and shear stresses for elastic core can be represented by (Arefi *et al*. 2018, Arefi and Zenkour 2017a, b)

$$\begin{aligned} (1-\xi^2\nabla^2)\sigma_\theta^c &= C_{\theta\theta}^c\,\varepsilon_\theta, \\ (1-\xi^2\nabla^2)\tau_{r\theta}^c &= C_{r\theta}^c\,\gamma_{r\theta}, \end{aligned} \tag{3}$$

in which C_{ij}^c are stiffness coefficients of elastic core and ∇^2 denotes Laplace operator in polar coordinate system. Small scale coefficient is defined by $\xi = e_0 a$ in which e_0 is nonlocal material constant and determined from experimental or by dynamics simulations results and a define internal characteristic scale (Arefi *et al*. 2018, Arefi and Zenkour 2017e). The constitutive equations for piezomagnetic face-sheets are expressed as (Shi and Zhang 2008, Arefi 2014, Arefi and Zenkour 2017a, b)

$$\begin{aligned} (1-\xi^2\nabla^2)\sigma_\theta^p &= C_{\theta\theta}^p\,\varepsilon_\theta - e_{\theta\theta r}^p E_r - q_{\theta\theta r}^p H_r, \\ (1-\xi^2\nabla^2)\tau_{r\theta}^p &= C_{r\theta}^p\,\gamma_{r\theta} - e_{r\theta\theta}^p E_\theta - q_{r\theta\theta}^p H_\theta, \end{aligned} \tag{4}$$

in which C_{ij}^{p} are stiffness coefficients of elastic core. Also, e_{ij} represent piezoelectric coefficients, q_{ij} are piezo-magnetic coefficients, E_i and H_i denote electric and magnetic field components, respectively.

For calculation of stress in piezo-magnetic face-sheets, it is necessary to calculate electric and magnetic fields. Electric and magnetic fields are derived using electric and magnetic potentials as (Arefi 2014, Arefi and Zenkour 2017a, b, c)

$$\begin{aligned} E_r &= -\frac{\partial \breve{\psi}}{\partial r}, \quad E_\theta = -\frac{1}{r}\frac{\partial \breve{\psi}}{\partial \theta}, \\ H_r &= -\frac{\partial \breve{\phi}}{\partial r}, \quad H_\theta = -\frac{1}{r}\frac{\partial \breve{\phi}}{\partial \theta}. \end{aligned} \tag{5}$$

The electric and magnetic components are given by (Arefi 2014, Arefi and Zenkour 2017a, b, c)

$$\begin{aligned} \breve{\psi}(r,\theta) &= -\psi(\theta)\cos\left(\frac{\pi}{h_p}\rho\right) + \frac{2\psi_0}{h_p}\rho, \\ \breve{\phi}(r,\theta) &= -\phi(\theta)\cos\left(\frac{\pi}{h_p}\rho\right) + \frac{2\phi_0}{h_p}\rho, \end{aligned} \tag{6}$$

in which ψ_0 and ϕ_0 represent applied electric and magnetic potentials, $\rho = \zeta \pm \frac{h_e}{2} \pm \frac{h_p}{2}$ for upper and lower piezo-magnetic face-sheets. The substitution of electric and magnetic potentials into Eq. (6) yields

$$\begin{aligned} E_r &= -\left[\frac{\pi}{h_p}\psi\sin\left(\frac{\pi}{h_p}\rho\right) + \frac{2\psi_0}{h_p}\right], \\ E_\theta &= \frac{1}{r}\frac{\partial \psi}{\partial \theta}\cos\left(\frac{\pi}{h_p}\rho\right) \\ H_r &= -\left[\frac{\pi}{h_p}\phi\sin\left(\frac{\pi}{h_p}\rho\right) + \frac{2\phi_0}{h_p}\right], \\ H_\theta &= \frac{1}{r}\frac{\partial \phi}{\partial \theta}\cos\left(\frac{\pi}{h_p}\rho\right). \end{aligned} \tag{7}$$

The electric displacement and magnetic induction along radial and circumferential directions are obtained by (Arefi 2014, Arefi and Zenkour 2017a, b, c, d)

$$\begin{aligned} (1-\xi^2\nabla^2)D_r^p &= e_{r\theta\theta}^p\,\varepsilon_\theta + \epsilon_{rr}^p E_r + m_{rr}^p H_r, \\ (1-\xi^2\nabla^2)D_\theta^p &= e_{\theta r\theta}^p\,\gamma_{r\theta} + \epsilon_{\theta\theta}^p E_\theta + m_{\theta\theta}^p H_\theta, \\ (1-\xi^2\nabla^2)B_r^p &= q_{r\theta\theta}^p\,\varepsilon_\theta + m_{rr}^p E_r + \mu_{rr}^p H_r, \\ (1-\xi^2\nabla^2)B_\theta^p &= q_{\theta r\theta}^p\,\gamma_{r\theta} + m_{\theta\theta}^p E_\theta + \mu_{\theta\theta}^p H_\theta, \end{aligned} \tag{8}$$

in which m_{ij} and μ_{ij} are dielectric and electromagnetic coefficients. In this stage and applying Hamilton's principle $\int \delta(T-U+V)\mathrm{d}t = 0$ to obtain equations of motion. Variation of strain energy δU is given by

$$\begin{aligned} \delta U = \iiint_v \; & (\sigma_{\theta\theta}\,\delta\varepsilon_{\theta\theta} + \sigma_{r\theta}\,\delta\gamma_{r\theta} - D_r\delta E_r \\ & - D_\theta\delta E_\theta - B_r\delta H_r - B_\theta\delta H_\theta)\mathrm{d}V. \end{aligned} \tag{9}$$

Setting the volume element $\mathrm{dV} = \mathrm{brdr d\theta} = \mathrm{b}(\mathrm{R}+\zeta)\mathrm{d}\zeta\mathrm{d}\theta$ in the above equations gives

$$\begin{aligned} \delta U = \iint_A \; & \Big[\sigma_{\theta\theta}\left(\frac{\delta u_r}{R+\zeta} + \frac{1}{R+\zeta}\frac{d\delta u_\theta}{d\theta} + \frac{\zeta}{R+\zeta}\frac{d\delta\chi}{d\theta}\right) \\ & + \sigma_{r\theta}\left(\frac{1}{R+\zeta}\frac{d\delta u_r}{d\theta} + \delta\chi - \frac{\delta u_\theta}{R+\zeta} \right. \\ & \left. - \frac{\zeta}{R+\zeta}\delta\chi\right) + D_r\frac{\pi}{h_p}\delta\psi\sin\left(\frac{\pi}{h_p}\rho\right) \\ & - D_\theta\frac{1}{r}\frac{d\delta\psi}{d\theta}\cos\left(\frac{\pi}{h_p}\rho\right) \\ & + B_r\frac{\pi}{h_p}\delta\phi\sin\left(\frac{\pi}{h_p}\rho\right) \\ & - B_\theta\frac{1}{r}\frac{d\delta\phi}{d\theta}cos\left(\frac{\pi}{h_p}\rho\right)\Big](R \\ & + \zeta)\mathrm{d}\zeta\mathrm{d}\theta, \end{aligned} \tag{10}$$

or

$$\begin{aligned} \delta U = \int \Big[& N_{\theta\theta}\,\delta u_r - N_{r\theta}\,\delta u_\theta + (RN_{r\theta} + M_{r\theta})\delta\chi \\ & - M_{r\theta}\,\delta\chi + \bar{D}_r\delta\psi \\ & + \bar{B}_r\delta\phi + N_{\theta\theta}\frac{d\delta u_\theta}{d\theta} + N_{r\theta}\frac{d\delta u_r}{d\theta} \\ & + M_{\theta\theta}\frac{d\delta\chi}{d\theta} - \bar{D}_\theta\frac{d\delta\psi}{d\theta} - \bar{B}_\theta\frac{d\delta\phi}{d\theta}\Big]\mathrm{d}\theta, \end{aligned} \tag{11}$$

where resultant components may be expressed by (Arefi 2014, Arefi and Zenkour 2017a, b, c)

$$\begin{aligned} \{N_{\theta\theta}, N_{r\theta}\} = & \int_{-\frac{h_e}{2}-h_p}^{-\frac{h_e}{2}} \{\sigma_{\theta\theta}, \sigma_{r\theta}\}d\zeta + \int_{-\frac{h_e}{2}}^{\frac{h_e}{2}} \{\sigma_{\theta\theta}, \sigma_{r\theta}\}d\zeta \\ & + \int_{\frac{h_e}{2}}^{\frac{h_e}{2}+h_p} \{\sigma_{\theta\theta}, \sigma_{r\theta}\}d\zeta, \end{aligned} \tag{12a}$$

$$\begin{aligned} \{M_{\theta\theta}, M_{r\theta}\} = & \int_{-\frac{h_e}{2}-h_p}^{-\frac{h_e}{2}} \zeta\{\sigma_{\theta\theta}, \sigma_{r\theta}\}d\zeta \\ & + \int_{-\frac{h_e}{2}}^{\frac{h_e}{2}} \zeta\{\sigma_{\theta\theta}, \sigma_{r\theta}\}d\zeta \\ & + \int_{\frac{h_e}{2}}^{\frac{h_e}{2}+h_p} \zeta\{\sigma_{\theta\theta}, \sigma_{r\theta}\}d\zeta, \end{aligned} \tag{12b}$$

$$\begin{aligned} \{\bar{D}_r, \bar{B}_r\} = & \int_{-\frac{h_e}{2}-h_p}^{-\frac{h_e}{2}} (R+\zeta)\frac{\pi}{h_p}sin\left(\frac{\pi}{h_p}\rho\right)\{D_r, B_r\}d\zeta \\ & + \int_{\frac{h_e}{2}}^{\frac{h_e}{2}+h_p} (R \\ & + \zeta)\frac{\pi}{h_p}sin\left(\frac{\pi}{h_p}\rho\right)\{D_r, B_r\}d\zeta, \end{aligned} \tag{12c}$$

$$\{\bar{D}_\theta, \bar{B}_\theta\} = \int_{-\frac{h_e}{2}-h_p}^{-\frac{h_e}{2}} cos\left(\frac{\pi}{h_p}\rho\right)\{D_r, B_r\}d\zeta \tag{12d}$$

$$+\int_{\frac{h_e}{2}}^{\frac{h_e}{2}+h_p} cos\left(\frac{\pi}{h_p}\rho\right)\{D_r, B_r\}d\zeta. \quad (12d)$$

Applying the integration by part yields on Eq. (11) leads to

$$\delta U = \int \begin{bmatrix} \left(N_{\theta\theta} - \frac{dN_{r\theta}}{d\theta}\right)\delta u_r - \left(N_{r\theta} + \frac{dN_{\theta\theta}}{d\theta}\right)\delta u_\theta \\ + \left(RN_{r\theta} - \frac{dM_{\theta\theta}}{d\theta}\right)\delta\chi + \left(\bar{D}_r + \frac{d\bar{D}_\theta}{d\theta}\right)\delta\psi \\ + \left(\bar{B}_r + \frac{d\bar{B}_\theta}{d\theta}\right)\delta\phi \end{bmatrix} d\theta. \quad (13)$$

Also, variation of energy due to external works is expressed as

$$\delta V = \iint_A \left(R_f - q\right)\delta u_r dA, \quad (14)$$

in which R_f is reaction of Pasternak's foundation represented by

$$R_f = K_1 u_r - K_2 \nabla^2 u_r, \quad (15)$$

where K_1 and K_2 represent spring and shear parameters of foundation. Applying $\nabla^2 = \frac{1}{r^2}\frac{\partial^2}{\partial\theta^2}$ into above equation, we will have the reaction of foundation as follows

$$R_f = K_1 u_r - K_2 \frac{1}{r^2}\frac{\partial^2 u_r}{\partial\theta^2}. \quad (16)$$

Also, the variation of kinetic energy is represented by

$$\delta T = \iint_A \rho[\dot{u}_r\delta\dot{u}_r + (\dot{u}_\theta + \zeta\dot{\chi})(\delta\dot{u}_\theta + \zeta\delta\dot{\chi})]b(R+\zeta)d\zeta d\theta. \quad (17)$$

Integration by part yields

$$\delta T = \int \begin{bmatrix} -A_1\ddot{u}_r\delta u_r - A_1\ddot{u}_\theta\delta u_\theta \\ -A_2\ddot{\chi}\delta u_\theta - A_2\ddot{u}_\theta\delta\chi - A_3\ddot{\chi}\delta\chi \end{bmatrix} d\theta, \quad (18)$$

in which the integration constants A_i are expressed in Appendix.

The formula of Hamilton's principle $\int \delta(T - U + V)\mathrm{d}t = 0$ leads to five governing equations of motion

$$\delta u_r: \; -N_{\theta\theta} + \frac{dN_{r\theta}}{d\theta} + \left(K_1 u_r - K_2 \frac{1}{\left(R - \frac{h_e}{2} - h_p\right)^2}\frac{d^2 u_r}{d\theta^2} - q\right) = A_1\ddot{u}_r, \quad (19a)$$

$$\delta u_\theta: \; \frac{dN_{\theta\theta}}{d\theta} + N_{r\theta} = A_1\ddot{u}_\theta + A_2\ddot{\chi}, \quad (19b)$$

$$\delta\chi: \; \frac{dM_{\theta\theta}}{d\theta} - RN_{r\theta} = A_2\ddot{u}_\theta + A_3\ddot{\chi}, \quad (19c)$$

$$\delta\psi: \; \bar{D}_r + \frac{d\bar{D}_\theta}{d\theta} = 0, \quad (19d)$$

$$\delta\phi: \; \bar{B}_r + \frac{d\bar{B}_\theta}{d\theta} = 0. \quad (19e)$$

In this stage, we can calculate the resultant components in terms of displacement and rotation components and electric and magnetic potentials. These resultants are defined as

$$\begin{aligned} (1-\xi^2\nabla^2)N_{\theta\theta} &= A_4 u_r + A_4\frac{du_\theta}{d\theta} + A_5\frac{d\chi}{d\theta} + A_6\psi \\ &\quad + N_\psi + A_7\phi + N_\phi, \\ (1-\xi^2\nabla^2)M_{\theta\theta} &= A_5 u_r + A_5\frac{du_\theta}{d\theta} + A_8\frac{d\chi}{d\theta} + A_9\psi \\ &\quad + M_\psi + A_{10}\phi + M_\phi, \\ (1-\xi^2\nabla^2)N_{r\theta} &= A_{11}\frac{du_r}{d\theta} + A_{12}\chi - A_{11}u_\theta - A_{13}\chi \\ &\quad - A_{14}\frac{d\psi}{d\theta} - A_{15}\frac{d\phi}{d\theta}, \end{aligned} \quad (20)$$

$$\begin{aligned} (1-\xi^2\nabla^2)\bar{D}_r &= A_{16}u_r + A_{16}\frac{du_\theta}{d\theta} + A_{17}\frac{d\chi}{d\theta} - A_{18}\psi \\ &\quad - D_\psi - A_{19}\phi - D_\phi, \\ (1-\xi^2\nabla^2)\bar{D}_\theta &= A_{23}\frac{du_r}{d\theta} + A_{24}\chi - A_{23}u_\theta - A_{25}\chi \\ &\quad + A_{29}\frac{d\psi}{d\theta} + A_{30}\frac{d\phi}{d\theta}, \end{aligned} \quad (21)$$

$$\begin{aligned} (1-\xi^2\nabla^2)\bar{B}_r &= A_{20}u_r + A_{20}\frac{du_\theta}{d\theta} + A_{21}\frac{d\chi}{d\theta} - A_{19}\psi \\ &\quad - B_\psi - A_{22}\phi - B_\phi, \\ (1-\xi^2\nabla^2)\bar{B}_\theta &= A_{26}\frac{du_r}{d\theta} + A_{27}\chi - A_{26}u_\theta - A_{28}\chi \\ &\quad + A_{30}\frac{d\psi}{d\theta} + A_{31}\frac{d\phi}{d\theta}, \end{aligned} \quad (22)$$

in which the integration constants are expressed in Appendix. Using the above resultant components into the equations of motion gives

$$\begin{aligned} &\delta u_r: \\ &A_{11}\frac{d^2u_r}{d\theta^2} - A_4 u_r - (A_4 + A_{11})\frac{du_\theta}{d\theta} \\ &+(A_{12} - A_{13} - A_5)\frac{d\chi}{d\theta} - A_{14}\frac{d^2\psi}{d\theta^2} - A_6\psi - A_{15}\frac{d^2\phi}{d\theta^2} \\ &-A_7\phi + (1-\xi^2\nabla^2)\left(K_1 u_r - K_2\frac{1}{r^2}\frac{d^2u_r}{d\theta^2} - q\right) \\ &= (1-\xi^2\nabla^2)\left(A_1\ddot{u}_r + N_\psi + N_\phi\right), \end{aligned} \quad (23)$$

$$\begin{aligned} &\delta u_\theta: \\ &(A_4 + A_{11})\frac{du_r}{d\theta} + A_4\frac{d^2u_\theta}{d\theta^2} - A_{11}u_\theta + A_5\frac{d^2\chi}{d\theta^2} \\ &+(A_{12} - A_{13})\chi + (A_6 - A_{14})\frac{d\psi}{d\theta} + (A_7 - A_{15})\frac{d\phi}{d\theta} \\ &= (1-\xi^2\nabla^2)\left(A_1\ddot{u}_\theta + A_2\ddot{\chi} - \frac{dN_\psi}{d\theta} - \frac{dN_\phi}{d\theta}\right), \end{aligned} \quad (24)$$

$\delta\chi$:

$$\begin{aligned}&(A_5 - RA_{11})\frac{du_r}{d\theta} + A_5\frac{d^2u_\theta}{d\theta^2} + RA_{11}u_\theta\\&+A_8\frac{d^2\chi}{d\theta^2} - R(A_{12} - A_{13})\chi + (A_9 + RA_{14})\frac{d\psi}{d\theta}\\&+(A_{10} + RA_{15})\frac{d\phi}{d\theta}\\&= (1 - \xi^2\nabla^2)\left(A_2\ddot{u}_\theta + A_3\ddot{\chi} - \frac{dM_\psi}{d\theta} - \frac{dM_\phi}{d\theta}\right),\end{aligned} \tag{25}$$

$\delta\psi$:

$$\begin{aligned}&-A_{23}\frac{d^2u_r}{d\theta^2} - A_{16}u_r + (A_{23} - A_{16})\frac{du_\theta}{d\theta}\\&+(A_{25} - A_{17} - A_{24})\frac{d\chi}{d\theta} - A_{29}\frac{d^2\psi}{d\theta^2} + A_{18}\psi\\&-A_{30}\frac{d^2\phi}{d\theta^2} + A_{19}\phi = -(1 - \xi^2\nabla^2)\left(\bar{D}_\psi + \bar{D}_\phi\right),\end{aligned} \tag{26}$$

$$\begin{aligned}&-A_{26}\frac{d^2u_r}{d\theta^2} - A_{20}u_r + (A_{26} - A_{20})\frac{du_\theta}{d\theta}\\&+(A_{28} - A_{21} - A_{27})\frac{d\chi}{d\theta} - A_{30}\frac{d^2\psi}{d\theta^2} + A_{19}\psi\\&-A_{31}\frac{d^2\phi}{d\theta^2} + A_{22}\phi = -(1 - \xi^2\nabla^2)\left(B_\psi + B_\phi\right).\end{aligned} \tag{27}$$

3. Solution procedure

Here, the free vibration and electro-magneto-mechanical bending results are presented. The proposed solutions for a simply-supported curved sandwich beam are given by

$$\begin{Bmatrix}(u_\theta, \chi)\\(u_r, \psi, \phi)\end{Bmatrix} = \mathrm{e}^{i\omega t}\sum_{m=1,3,5}^{N}\begin{Bmatrix}(U_\theta, X)\cos(\beta_1\theta)\\(U_r, \Psi, \Phi)\sin(\beta_1\theta)\end{Bmatrix}, \tag{28}$$

in which $\beta_1 = m\pi$. The proposed solution will be used into the equations of motion to obtain

$$[K]\{X\} = \{F\} + \omega^2[M]\{X\}, \tag{29}$$

where $\{X\} = \{U_r, U_\theta, X, \Psi, \Phi\}$ represents an unknown vector. The symmetric elements of matrix $[K]$ and $[M]$ are represented by

$$\begin{aligned}&K_{11} = -A_{11}\beta_1^2 - A_4 + K_1 + K_2\frac{1}{\left(R - \frac{h}{2} - \frac{h_p}{2}\right)^2}\beta_1^2,\\&K_{12} = (A_4 + A_{11})\beta_1, \quad K_{13} = (A_5 - A_{12} + A_{13})\beta_1,\\&K_{14} = A_{14}\beta_1^2 - A_6, \quad K_{15} = A_{15}\beta_1^2 - A_7,\\&M_{11} = A_1, \quad K_{21} = (A_4 + A_{11})\beta_1,\\&K_{22} = -A_4\beta_1^2 - A_{11}, \quad K_{23} = -A_5\beta_1^2 + A_{12} - A_{13},\\&K_{24} = (A_6 - A_{14})\beta_1, \quad K_{25} = (A_7 - A_{15})\beta_1,\\&M_{22} = A_1, \quad M_{23} = A_2, \quad K_{31} = (A_5 - RA_{11})\beta_1,\\&K_{32} = -A_5\beta_1^2 + RA_{11},\\&K_{33} = -A_8\beta_1^2 - R(A_{12} - A_{13})\chi,\\&K_{34} = (A_9 + RA_{14})\beta_1, \quad K_{35} = (A_{10} + RA_{15})\beta_1,\\&M_{32} = A_2, \quad M_{33} = A_3, \quad K_{41} = A_{23}\beta_1^2 - A_{16},\\&K_{42} = (A_{16} - A_{23})\beta_1, \quad K_{43} = (A_{17} + A_{24} - A_{25})\beta_1,\\&K_{44} = A_{29}\beta_1^2 + A_{18}, \quad K_{45} = A_{30}\beta_1^2 + A_{19},\\&K_{51} = A_{26}\beta_1^2 - A_{20}u_r, \quad K_{52} = (A_{20} - A_{26})\beta_1,\\&K_{53} = (A_{21} + A_{27} - A_{28})\beta_1,\\&K_{54} = A_{30}\beta_1^2 + A_{19}, \quad K_{55} = A_{31}\beta_1^2 + A_{22}.\end{aligned} \tag{30}$$

Also, elements of force vector $\{F\}$ are given by

$$\begin{aligned}&F_1 = N_\psi + N_\phi - R_f + q, \quad F_2 = -\frac{dN_\psi}{d\theta} - \frac{dN_\phi}{d\theta},\\&F_3 = -\frac{dM_\psi}{d\theta} - \frac{dM_\phi}{d\theta}, \quad F_4 = -D_\psi - D_\phi,\\&F_5 = -B_\psi - B_\phi.\end{aligned} \tag{31}$$

4. Results and discussions

Here, numerical results of the current problem are presented. Material properties of elastic core and piezomagnetic layers must be introduced (Hou and Leung 2004).

Core

$$E = 210\ \text{GPa}, \quad v = 0.3. \tag{32}$$

Piezomagnetic face-sheets

$$\begin{aligned}&C_{\theta\theta}^p = 286\ \text{GPa}, \quad C_{r\theta}^p = 45.3\ \text{GPa},\\&e_{\theta\theta r}^p = e_{r\theta\theta}^p = -4.4\ (\text{C/m}^2),\\&e_{\theta\theta\theta}^p = e_{\theta r\theta}^p = 11.6\ (\text{C/m}^2),\\&q_{\theta\theta r}^p = q_{r\theta\theta}^p = 580.3\ (\text{N/Am}),\\&q_{\theta\theta\theta}^p = q_{\theta r\theta}^p = 550\ (\text{N/Am}),\\&\epsilon_{rr}^p = 9.3\times10^{-11}\ (\text{C/mV}),\\&\epsilon_{\theta\theta}^p = 8\times10^{-11}\ (\text{C/mV}),\\&m_{rr}^p = 3\times10^{-12}\ (\text{Ns/CV}),\\&m_{\theta\theta}^p = 5\times10^{-12}\ (\text{Ns/CV}),\\&\mu_{rr}^p = 1.57\times10^{-4}\ (\text{Ns}^2/\text{C}^2),\\&\mu_{\theta\theta}^p = -5.9\times10^{-4}\ (\text{Ns}^2/\text{C}^2).\end{aligned} \tag{33}$$

4.1 Free vibration responses

Here, results of free vibration analysis are presented. For this purpose, the characteristic equation of Eq. (22) with ignore of force term is solved. Fig. 2 shows the fundamental natural frequencies of curved nanobeam in terms of two parameters of Pasternak's foundation K_1 and K_2. It is observed that increase of spring and shear parameters of foundation increases the fundamental natural frequencies of curved nanobeam because of increase of stiffness of foundation.

Fig. 3 shows variation of fundamental natural frequencies of curved nanobeam in terms of nonlocal parameter for various values of radius of curvature. It can

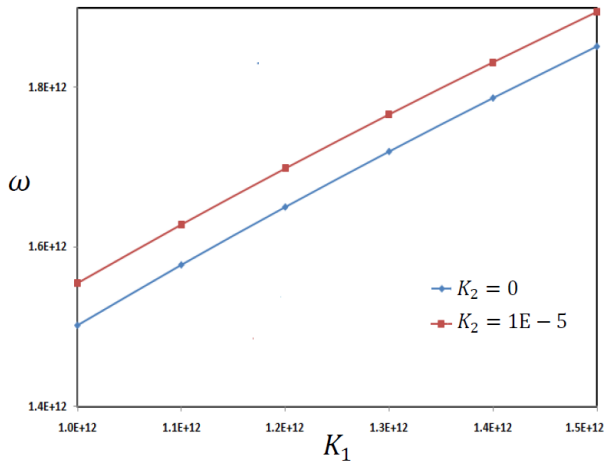

Fig. 2 The fundamental natural frequencies of sandwich curved beam in terms of two parameters of Pasternak's foundation K_1 and K_2

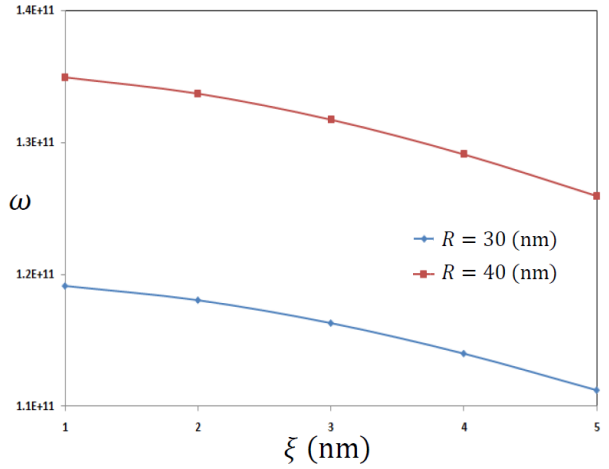

Fig. 3 The fundamental natural frequencies of sandwich curved beam in terms of nonlocal parameter for two values of radius of curvature

be observed that the increase in nonlocal parameter reduces stiffness of nanobeam and consequently leads to lower natural frequencies. This conclusion is based on the results of previous works (Arefi and Zenkour 2017a, b, c) and is in good agreement. In addition, it is observed that natural frequencies are increased with increase of radius of curvature. It can be concluded that increase of radius of curvature leads to significant increase of stiffness of curved beam.

4.2 The influence of radius of curvature

The innovation of this paper is discussion on the influence of various radii of curvature R on the bending electro-magnetic results of the curved beam. The current discussion can present important results to guide designer or engineers for selection and design of curved sensors and actuators.

Fig. 4 depicts the variation of non-dimensional radial $\bar{u}_r = \frac{u_r}{h}$ and circumferential $\bar{u}_\theta = \frac{u_\theta}{h}$ displacements and rotation χ in terms of various radii of curvature R. It can be concluded that the mentioned displacement and component rotations are decreased with increase of radius of curvature R. The reason of this decrease is increase of stiffness of curved beam due to increase of radius of curvature R. In addition, it is concluded that the magnitude of radial deformation is greater than circumferential displacement because of existence of direct radial force along the radial direction.

Fig. 5 depicts the maximum electric ψ and magnetic $\bar{\phi} = 10^3\phi$ potentials through thickness direction in terms of various radii of curvature R. the numerical results indicate that increase of radii of curvature slightly decrease maximum electric and magnetic potentials. The author can conclude that increase of radius of curvature leads to increase of stiffness of curved beam and consequently decrease of maximum electric and magnetic potentials.

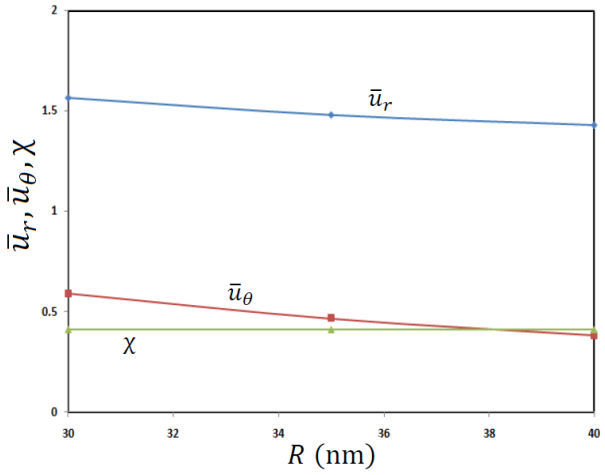

Fig. 4 The non-dimensional radial $\bar{u}_r$ and circumferential $\bar{u}_\theta$ displacements and rotation χ in terms of various radii of curvature R

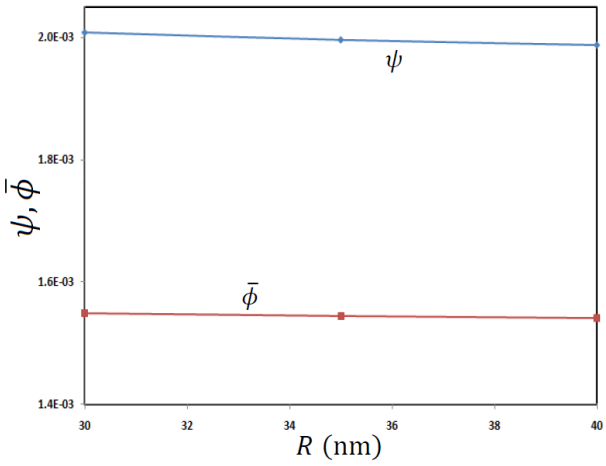

Fig. 5 The maximum electric ψ and magnetic $\bar{\phi}$ potentials through thickness direction in terms of various radii of curvature R

4.3 The influence of nonlocal parameter

The influence of nonlocal parameter ξ can be investigated on the magneto-electro-elastic results of the curved beam. Fig. 6 shows that how non-dimensional radial $\bar{u}_r$ and circumferential $\bar{u}_\theta$ displacements and rotation χ changes with increase of nonlocal parameter ξ. We can conclude that increase of nonlocal parameter decreases stiffness of curved beam and finally increases non-dimensional radial and circumferential displacements and rotation. Increase of displacement and then decrease of stiffness of curved beam with increase of nonlocal parameter is in accordance with conclusion of literatures (Arefi and Zenkour 2017a, b, c).

Shown in Fig. 7 is maximum electric ψ and magnetic $\bar{\phi}$ potentials through thickness direction in terms of nonlocal parameter ξ. The obtained results indicate that increase of nonlocal parameter of structure significantly increases maximum electric and magnetic potentials. One can conclude that with increase of nonlocal parameter, the stiffness of nano materials are decreased that leads to increase of deformations and maximum electric and magnetic potentials.

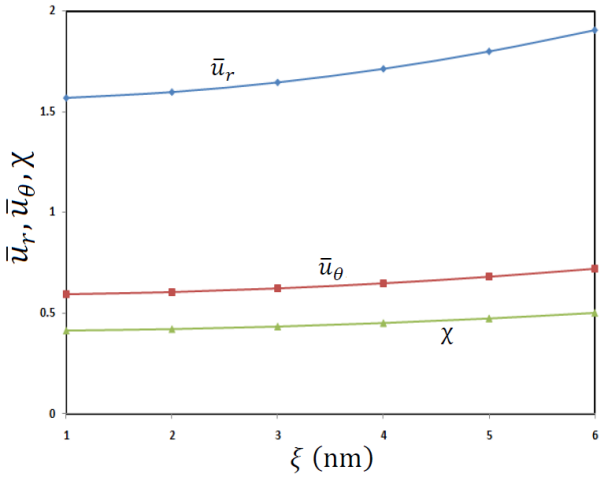

Fig. 6 The non-dimensional radial $\bar{u}_r$ and circumferential $\bar{u}_\theta$ displacements and rotation χ in terms of nonlocal parameter ξ

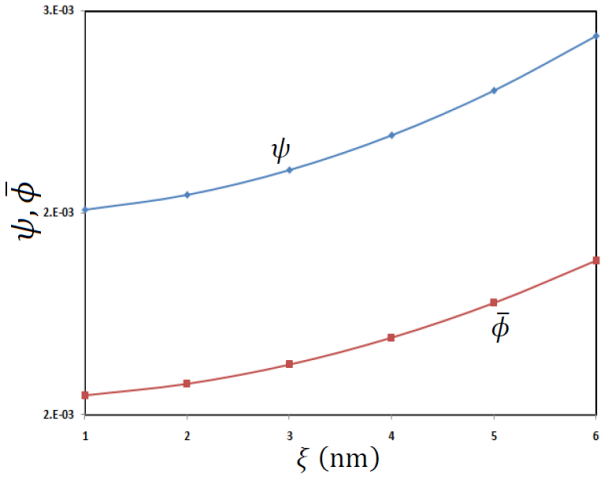

Fig. 7 The maximum electric ψ and magnetic $\bar{\phi}$ potentials through thickness direction in terms of nonlocal parameter ξ

4.4 The influence of electromagnetic loadings

Shown in Fig. 8 is the non-dimensional value of radial displacement $\bar{u}_r$ in terms of applied electric and magnetic potentials ψ_0 and ϕ_0. The numerical results in this figure indicates that increase of applied electric potential ψ_0 leads to increase of radial displacement while increase of applied magnetic potential ϕ_0 leads to decrease of radial displacement. The influences of applied electric and magnetic potentials ψ_0 and ϕ_0 on the non-dimensional value of circumferential displacement $\bar{u}_\theta$ are depicted in Fig. 9. The similar behavior expressed for Fig. 8 can be presented for Fig. 9. Shown in Fig. 10 is rotation of curved nanobeam χ in terms of applied electric and magnetic potentials ψ_0 and ϕ_0. One can see that behavior of electro-magnetic structures due to applied electric and magnetic potentials are in good agreement with results of

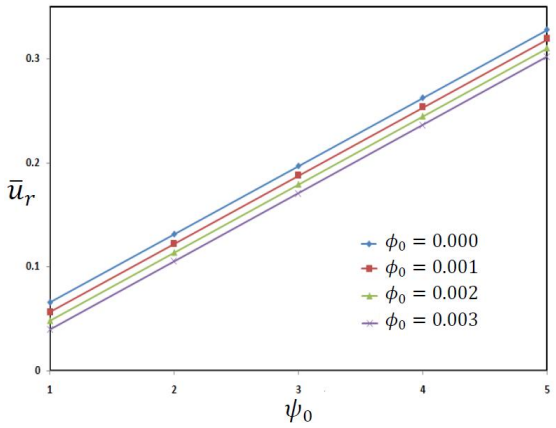

Fig. 8 The non-dimensional value of radial displacement $\bar{u}_r$ in terms of applied electric ψ_0 and magnetic ϕ_0 potentials

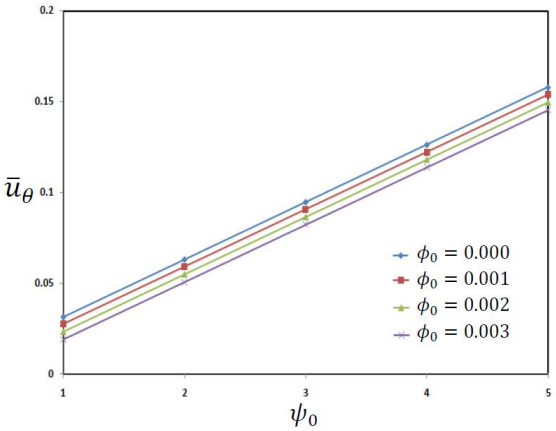

Fig. 9 The non-dimensional value of circumferential displacement $\bar{u}_\theta$ in terms of applied electric ψ_0 and magnetic ϕ_0 potentials

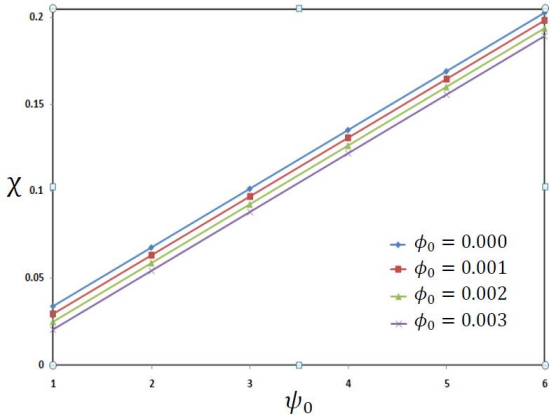

Fig. 10 The rotation χ of curved beam in terms of applied electric ψ_0 and magnetic ϕ_0 potentials

literature (Arefi and Zenkour 2017a, b, c).

The maximum value of electric and magnetic potentials ψ and ϕ through thickness direction in terms of applied electric and magnetic potentials ψ_0 and ϕ_0 is presented in Figs. 11 and 12. It can be concluded that increase of applied electric potential and decrease of applied magnetic potential increases maximum electric and magnetic potentials of curved piezo-magnetic face-sheets.

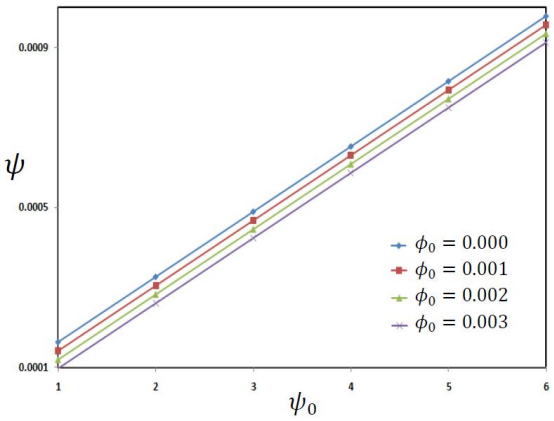

Fig. 11 Maximum electric potential ψ through thickness direction in terms of applied electric ψ_0 and magnetic ϕ_0 potentials

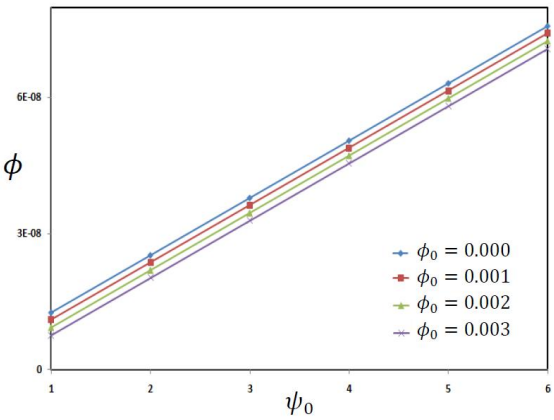

Fig. 12 Maximum magnetic potential ϕ through thickness direction in terms of applied electric ψ_0 and magnetic ϕ_0 potentials

4.5 The influence of two parameters of Pasternak's foundation

Figs. 13 and 14 shows the variation of dimensionless value of radial $\bar{u}_r$ and circumferential $\bar{u}_\theta$ displacements in terms of two parameters of Pasternak's foundation K_1 and K_2. It is observed that radial and circumferential displacements are decreasing uniformly with increase of both parameters. This decrease is due to increase of stiffness of foundation. Fig. 15 shows variation of rotation of nanobeam in terms of two parameters of foundation. Figs. 16 and 17 show the variation of maximum electric and magnetic potentials in terms of two parameters of foundation. It is concluded that maximum electric and magnetic potential are decreased with increasing the spring and shear parameters of foundation.

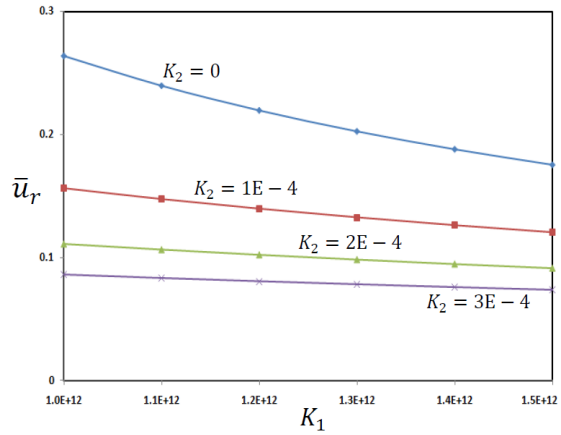

Fig. 13 Dimensionless radial displacement $\bar{u}_r$ in terms of two parameters of Pasternak's foundation K_1 and K_2

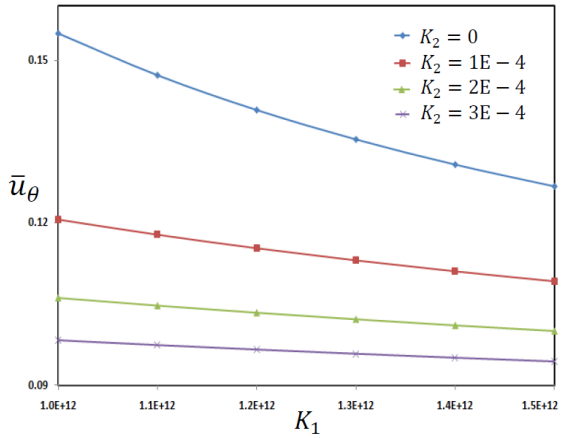

Fig. 14 Dimensionless circumferential displacement $\bar{u}_\theta$ in terms of two parameters of Pasternak's foundation K_1 and K_2

4.6 Two-dimensional presentation of results

Two-dimensional distribution of dimensionless value of radial $\bar{u}_r$ and circumferential $\bar{u}_\theta$ displacements in terms of applied electric potential and nonlocal parameter can be displayed in Figs. 18 and 19.

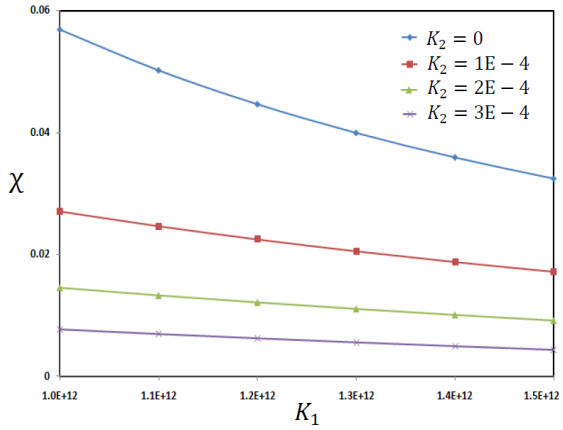

Fig. 15 The rotation χ of curved beam in terms of two parameters of Pasternak's foundation K_1 and K_2

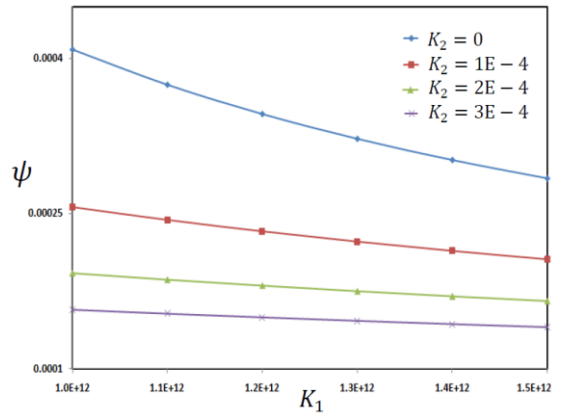

Fig. 16 Maximum electric potential ψ through thickness direction in terms of two parameters of Pasternak's foundation K_1 and K_2

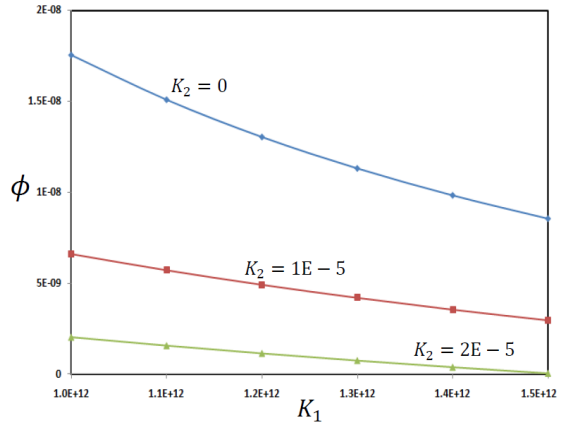

Fig. 17 Maximum magnetic potential ϕ through thickness direction in terms of two parameters of Pasternak's foundation K_1 and K_2

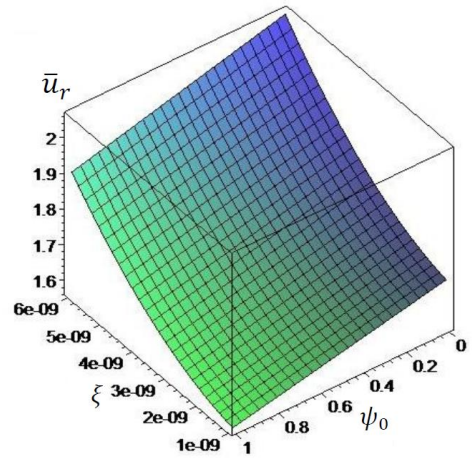

Fig. 18 Two-dimensional distribution of the non-dimensional radial displacement $\bar{u}_r$ in terms of nonlocal parameter ξ and applied electric potential ψ_0

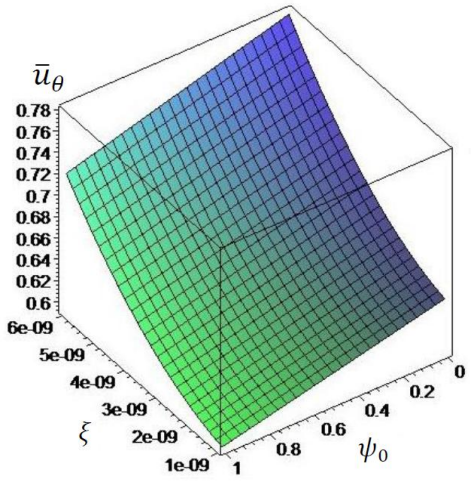

Fig. 19 Two-dimensional distribution of dimensionless circumferential displacement $\bar{u}_\theta$ in terms of nonlocal parameter ξ and applied electric potential ψ_0

5. Conclusions

In this paper, based on first-order theory and nonlocal piezoelectricity, equations of motion for a curved three-layer nanobeam including an elastic core and two curved piezo-magnetic face-sheets were presented. The piezo-magnetic face-sheets under applied electric and magnetic potentials. The analytical solution was presented for a simply-supported curved nanobeam. The numerical results show that some important parameters have significant influence on vibration and bending behaviors of curved nanobeam. The important conclusions are expressed as:

(1) As most important parameter in analysis of curved nanobeam, the influence of radius of curvature was studied. The numerical results indicate that with increase of radius or curvature, the stiffness of curved nanobeam are increased. Due to this increasing, the fundamental frequencies are increased and bending results are decreased significantly.
(2) Nonlocal parameter of nanobeam can significantly change the behavior of structure. It is concluded that with increase of nonlocal parameter, fundamental frequencies are decreased and bending results are decrease. This is due to decrease of stiffness with increase of nonlocal parameter.
(3) The influence of spring and shear parameters of foundation was discussed on the fundamental frequencies and bending results of curved nanobeam. The numerical results indicate that fundamental frequencies are increased with increase of both parameters of foundation due to increase of foundation. Furthermore, the radial and circumferential displacements, rotation and electric and magnetic potentials are decrease.
(4) Piezomagnetic face-sheets can be subjected to applied electric and magnetic potential. These parameters of loading can control the displacements or stresses in curved beam. The numerical results indicate that increase of applied electric potential increases all mechanical, electrical and magnetic components. Furthermore, it can be concluded that increase of magnetic potential decrease electro-magneto-mechanical components.

References

Amar, L.H.H., Kaci, A., Yeghnem, R. and Tounsi, A. (2018), "A new four-unknown refined theory based on modified couple stress theory for Size-dependent bending and vibration analysis of functionally graded", *Steel Compos. Struct., Int. J.*, **26**(1), 89-102.

Arefi, M. (2014), "A complete set of equations for piezo-magnetoelastic analysis of a functionally graded thick shell of revolution", *Latin Am. J. Solids Struct.*, **11**(11), 2073-2092.

Arefi, M. (2015), "Elastic solution of a curved beam made of functionally graded materials with different cross sections", *Steel Compos. Struct., Int. J.*, **18**(3), 659-672.

Arefi, M. and Rahimi, G.H. (2014), "Application of shear deformation theory for two dimensional electro-elastic analysis of a FGP cylinder", *Smart Struct. Syst., Int. J.*, **13**(1), 1-24.

Arefi, M. and Zenkour, A.M. (2017a), "Size-dependent vibration and bending analyses of the piezomagnetic three-layer nanobeams", *Appl. Phys. A*, **123**(3), 202.

Arefi, M. and Zenkour, A.M. (2017b), "Effect of thermo-magneto-electro-mechanical fields on the bending behaviors of a three-layered nanoplate based on sinusoidal shear-deformation plate theory", *J. Sandw. Struct. Mater.* DOI: 1099636217697497

Arefi, M. and Zenkour, A.M. (2017c), "Employing the coupled stress components and surface elasticity for nonlocal solution of wave propagation of a functionally graded piezoelectric Love nanorod model", *J. Intel. Mater. Syst. Struct.*, **28**(17), 2403-2413.

Arefi, M. and Zenkour, A.M. (2017d), "Size-dependent free vibration and dynamic analyses of piezo-electro-magnetic sandwich nanoplates resting on viscoelastic foundation", *Phys. B: Cond. Mat.*, **521**, 188-197.

Arefi, M. and Zenkour, A.M. (2017e), "Influence of magneto-electric environments on size-dependent bending results of three-layer piezomagnetic curved nanobeam based on sinusoidal shear deformation theory", *J. Sandw. Struct. Mater.* DOI: 1099636217723186

Arefi, M. and Zenkour, A.M. (2017f), "Electro-magneto-elastic analysis of a three-layer curved beam", *Smart Struct. Syst., Int. J.*, **19**(6), 695-703.

Arefi, M., Zamani, M.H. and Kiani, M. (2018), "Size-dependent free vibration analysis of three-layered exponentially graded nanoplate with piezomagnetic face-sheets resting on Pasternak's foundation", *J. Intel. Mater. Syst. Struct.*, **29**(5), 774-786.

Arslan, E. and Usta, R. (2014), "Mechanical and electrical fields of piezoelectric curved sensors", *Arch. Mech.*, **66**(5), 329-342.

Bahadur, R., Upadhyay, A.K. and Shukla, K.K. (2017), "Static analysis of singly and doubly curved panels on rectangular plan-form", *Steel Compos. Struct., Int. J.*, **24**(6), 659-670.

Ebrahimi, F. and Barati, M.R. (2017), "A nonlocal strain gradient refined beam model for buckling analysis of size-dependent shear-deformable curved FG nanobeams", *Compos. Struct.*, **159**, 174-182.

Ebrahimi, N. and Beni, Y.T. (2016), "Electro-mechanical vibration of nanoshells using consistent size-dependent piezoelectric theory", *Steel Compos. Struct., Int. J.*, **22**(6), 1301-1336.

Hajianmaleki, M. and Qatu, M.S. (2013), "Vibrations of straight and curved composite beams: A review", *Compos. Struct.*, **100**, 218-232.

Hou, P.F. and Leung, A.Y.T. (2004), "The transient responses of magneto-electro-elastic hollow cylinders", *Smart Mater. Struct.*, **13**, 762-776.

Kakar, R. and Kakar, S. (2014), "Electro-magneto-thermoelastic surface waves in non-homogeneous orthotropic granular half space", *Geomech. Eng., Int. J.*, **7**(1), 1-36.

Kakar, R. and Kakar, S. (2015), "Edge wave propagation in an electro-magneto-thermoelastic homogeneous plate subjected to stress", *Struct. Eng. Mech., Int. J.*, **53**(6), 1201-1214.

Koutsawa, Y. and Daya, E.M. (2007), "Static and free vibration analysis of laminated glass beam on viscoelastic supports", *Int. J. Solids Struct.*, **44**, 8735-8750.

Kuang, Y.D., Li, G.Q., Chen, C.Y. and Min, Q. (2007), "The static responses and displacement control of circular curved beams with piezoelectric actuators", *Smart Mater. Struct.*, **16**, 1016-1024.

Mohammadimehr, M. and Shahedi, S. (2016), "Nonlinear magneto-electro-mechanical vibration analysis of double-bonded sandwich Timoshenko microbeams based on MSGT using GDQM", *Steel Compos. Struct., Int. J.*, **21**(1), 1-36.

Pydah, A. and Sabale, A. (2017), "Static analysis of bi-directional functionally graded curved beams", *Compos. Struct.*, **160**, 867-876.

Rahmani, O., Deyhim S. and Hosseini, S.A.H. (2018), "Size dependent bending analysis of micro/nano sandwich structures based on a nonlocal high order theory", *Steel Compos. Struct., Int. J.*, **27**(3), 371-388.

Shao, D., Hu, S., Wang, Q. and Pang, F. (2016), "A unified analysis for the transient response of composite laminated curved beam with arbitrary lamination schemes and general boundary restraints", *Compos. Struct.*, **154**, 507-526.

Shi, Z.F. (2005), "Bending behavior of piezoelectric curved actuator", *Smart Mater. Struct.*, **14**, 835-842.

Shi, Z.F. and Zhang, T. (2008), "Bending analysis of a piezoelectric curved actuator with a generally graded property for the piezoelectric parameter", *Smart Mater. Struct.*, **17**, 045018, 7 pages.

Sun, D.C. and Tong, L. (2001), "Sensor/actuator equations for curved piezoelectric fibers and vibration control of composite beams using fiber modal actuators/sensors", *J. Sound Vib.*, **241**(2), 297-314.

Sun, D.C. and Tong, L. (2002), "Modeling and analysis of curved beams with debonded piezoelectric sensor/actuator patches", *Int. J. Mech. Sci.*, **44**, 1755-1777.

Susanto, K. (2009), "Vibration analysis of piezoelectric laminated slightly curved beams using distributed transfer function method", *Int. J. Solids Struct.*, **46**, 1564-1573.

Yan, Z. and Jiang, L. (2011), "Electromechanical response of a curved piezoelectric nanobeam with the consideration of surface effects", *J. Phys. D*, **44**, 365301, 8 pages.

Zhou, Y., Dong, Y. and Li, S. (2010), "Analysis of a curved beam MEMS piezoelectric vibration energy harvester", *Adv. Mater. Res.*, **139-141**, 1578-1581.

Zhou, Y., Nyberg, T.R., Xiong, G., Zhou, H. and Li, S. (2016), "Precise deflection analysis of laminated piezoelectric curved beam", *J. Intel. Mater. Syst. Struct.*, **27**(16), 2179-2198.

CC

Appendix

$$\{A_1, A_2, A_3\} = \int_{-\frac{h_e}{2}-h_p}^{-\frac{h_e}{2}} \rho(R+\zeta)\{1,\zeta,\zeta^2\}d\zeta + \int_{-\frac{h_e}{2}}^{\frac{h_e}{2}} \rho(R+\zeta)\{1,\zeta,\zeta^2\}d\zeta + \int_{\frac{h_e}{2}}^{\frac{h_e}{2}+h_p} \rho(R+\zeta)\{1,\zeta,\zeta^2\}d\zeta.$$

$$\{A_4, A_5, A_8\} = \int_{-\frac{h_e}{2}-h_p}^{-\frac{h_e}{2}} \frac{C^p_{\theta\theta}}{R+\zeta}\{1,\zeta,\zeta^2\}d\zeta + \int_{-\frac{h_e}{2}}^{\frac{h_e}{2}} \frac{C_{\theta\theta}}{R+\zeta}\{1,\zeta,\zeta^2\}d\zeta + \int_{\frac{h_e}{2}}^{\frac{h_e}{2}+h_p} \frac{C^p_{\theta\theta}}{R+\zeta}\{1,\zeta,\zeta^2\}d\zeta,$$

$$\{A_6, A_7, A_9, A_{10}\} = \int_{-\frac{h_e}{2}-h_p}^{-\frac{h_e}{2}} \frac{\pi}{h_p}\sin\left(\frac{\pi}{h_p}\rho\right)\{e^p_{\theta\theta r}, q^p_{\theta\theta r}, \zeta e^p_{\theta\theta r}, \zeta q^p_{\theta\theta r}\}d\zeta + \int_{\frac{h_e}{2}}^{\frac{h_e}{2}+h_p} \frac{\pi}{h_p}\sin\left(\frac{\pi}{h_p}\rho\right)\{e^p_{\theta\theta r}, q^p_{\theta\theta r}, \zeta e^p_{\theta\theta r}, \zeta q^p_{\theta\theta r}\}d\zeta,$$

$$\{A_{11}, A_{12}, A_{13}\} = \int_{-\frac{h_e}{2}-h_p}^{-\frac{h_e}{2}} \frac{C^p_{r\theta}}{R+\zeta}\{1,R+\zeta,\zeta^2\}d\zeta + \int_{-\frac{h_e}{2}}^{\frac{h_e}{2}} \frac{C_{r\theta}}{R+\zeta}\{1,R+\zeta,\zeta^2\}d\zeta + \int_{\frac{h_e}{2}}^{\frac{h_e}{2}+h_p} \frac{C^p_{r\theta}}{R+\zeta}\{1,R+\zeta,\zeta^2\}d\zeta,$$

$$\{A_{14}, A_{15}\} = \int_{-\frac{h_e}{2}-h_p}^{-\frac{h_e}{2}} \frac{\cos\left(\frac{\pi}{h_p}\rho\right)}{R+\zeta}\{e^p_{r\theta\theta}, q^p_{r\theta\theta}\}d\zeta + \int_{\frac{h_e}{2}}^{\frac{h_e}{2}+h_p} \frac{\cos\left(\frac{\pi}{h_p}\rho\right)}{R+\zeta}\{e^p_{r\theta\theta}, q^p_{r\theta\theta}\}d\zeta,$$

$$\{N_\psi, N_\phi, M_\psi, M_\phi\} = \int_{-\frac{h_e}{2}-h_p}^{-\frac{h_e}{2}} \left\{\frac{2\psi_0}{h_p}e^p_{\theta\theta\theta}, \frac{2\phi_0}{h_p}q^p_{\theta\theta\theta}, \frac{2\psi_0}{h_p}\zeta e^p_{\theta\theta\theta}, \frac{2\phi_0}{h_p}\zeta q^p_{\theta\theta\theta}\right\}d\zeta + \int_{\frac{h_e}{2}}^{\frac{h_e}{2}+h_p} \left\{\frac{2\psi_0}{h_p}e^p_{\theta\theta\theta}, \frac{2\phi_0}{h_p}q^p_{\theta\theta\theta}, \frac{2\psi_0}{h_p}\zeta e^p_{\theta\theta\theta}, \frac{2\phi_0}{h_p}\zeta q^p_{\theta\theta\theta}\right\}d\zeta,$$

$$\{A_{16}, A_{17}, A_{20}, A_{21}\} = \int_{-\frac{h_e}{2}-h_p}^{-\frac{h_e}{2}} \frac{\pi}{h_p}sin\left(\frac{\pi}{h_p}\rho\right)\{e^p_{r\theta\theta}, \zeta e^p_{r\theta\theta}, q^p_{r\theta\theta}, \zeta q^p_{r\theta\theta}\}d\zeta + \int_{\frac{h_e}{2}}^{\frac{h_e}{2}+h_p} \frac{\pi}{h_p}\sin\left(\frac{\pi}{h_p}\rho\right)\{e^p_{r\theta\theta}, \zeta e^p_{r\theta\theta}, q^p_{r\theta\theta}, \zeta q^p_{r\theta\theta}\}d\zeta,$$

$$\{A_{18}, A_{19}, A_{22}\} = \int_{-\frac{h_e}{2}-h_p}^{-\frac{h_e}{2}} (R+\zeta)\left[\frac{\pi}{h_p}\sin\left(\frac{\pi}{h_p}\rho\right)\right]^2\{\epsilon^p_{rr}, m^p_{rr}, \mu^p_{rr}\}d\zeta + \int_{\frac{h_e}{2}}^{\frac{h_e}{2}+h_p} (R+\zeta)\left[\frac{\pi}{h_p}\sin\left(\frac{\pi}{h_p}\rho\right)\right]^2\{\epsilon^p_{rr}, m^p_{rr}, \mu^p_{rr}\}d\zeta,$$

$$\{D_\psi, D_\phi, B_\psi, B_\phi\} = \int_{-\frac{h_e}{2}-h_p}^{-\frac{h_e}{2}} (R+\zeta)\left\{\frac{2\psi_0}{h_p}\epsilon^p_{rr}, \frac{2\phi_0}{h_p}m^p_{rr}, \frac{2\psi_0}{h_p}m^p_{rr}, \frac{2\phi_0}{h_p}\mu^p_{rr}\right\}d\zeta + \int_{\frac{h_e}{2}}^{\frac{h_e}{2}+h_p} (R+\zeta)\left\{\frac{2\psi_0}{h_p}\epsilon^p_{rr}, \frac{2\phi_0}{h_p}m^p_{rr}, \frac{2\psi_0}{h_p}m^p_{rr}, \frac{2\phi_0}{h_p}\mu^p_{rr}\right\}d\zeta,$$

$$\{A_{23}, A_{24}, A_{25}, A_{26}, A_{27}, A_{28}\} = \int_{-\frac{h_e}{2}-h_p}^{-\frac{h_e}{2}} \frac{\cos\left(\frac{\pi}{h_p}\rho\right)}{R+\zeta}\{e^p_{\theta r\theta}, (R+\zeta)e^p_{\theta r\theta}, \zeta e^p_{\theta r\theta}, q^p_{\theta r\theta}, (R+\zeta)q^p_{\theta r\theta}, \zeta q^p_{\theta r\theta}\}d\zeta + \int_{\frac{h_e}{2}}^{\frac{h_e}{2}+h_p} \frac{\cos\left(\frac{\pi}{h_p}\rho\right)}{R+\zeta}\{e^p_{\theta r\theta}, (R+\zeta)e^p_{\theta r\theta}, \zeta e^p_{\theta r\theta}, q^p_{\theta r\theta}, (R+\zeta)q^p_{\theta r\theta}, \zeta q^p_{\theta r\theta}\}d\zeta,$$

$$\{A_{29}, A_{30}, A_{31}\} = \int_{-\frac{h_e}{2}-h_p}^{-\frac{h_e}{2}} \frac{\cos^2\left(\frac{\pi}{h_p}\rho\right)}{R+\zeta}\{\epsilon^p_{\theta\theta}, m^p_{\theta\theta}, \mu^p_{\theta\theta}\}d\zeta + \int_{\frac{h_e}{2}}^{\frac{h_e}{2}+h_p} \frac{\cos^2\left(\frac{\pi}{h_p}\rho\right)}{R+\zeta}\{\epsilon^p_{\theta\theta}, m^p_{\theta\theta}, \mu^p_{\theta\theta}\}d\zeta.$$